Fiber-Based All-Solid-State Flexible Supercapacitors for Self-Powered Systems

Xu Xiao,[†] Tianqi Li,[†] Peihua Yang,[‡] Yuan Gao,[†] Huanyu Jin,[†] Weijian Ni,[†] Wenhui Zhan,[†] Xianghui Zhang,[†] Yuanzhi Cao,[†] Junwen Zhong,[†] Li Gong,[§] Wen-Chun Yen,[⊥] Wenjie Mai,[‡] Jian Chen,[§] Kaifu Huo,[†] Yu-Lun Chueh,[⊥] Zhong Lin Wang,[¶] and Jun Zhou[†,*]

[†]Wuhan National Laboratory for Optoelectronics (WNLO), and College of Optoelectronic Science and Engineering, Huazhong University of Science and Technology (HUST), Wuhan 430074, China, [‡]Department of Physics, Jinan University, Guangzhou 510632, China, [§]Instrumental Analysis & Research Center, Sun Yat-sen University, Guangzhou 510275, China, [⊥]Department of Materials Science and Engineering, National Tsinghua University, Hsinchu 30013, Taiwan, and [¶]School of Materials Science and Engineering, Georgia Institute of Technology, Atlanta, Georgia 30332-0245, United States

ABSTRACT

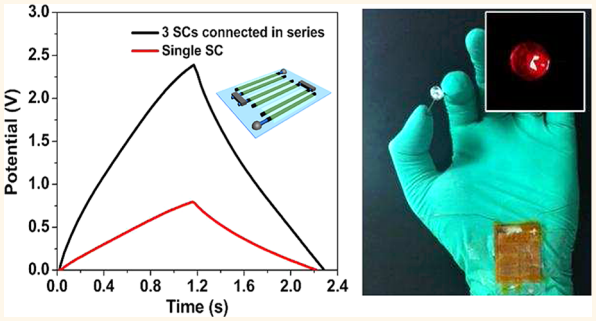

All-solid-state flexible supercapacitors based on a carbon/MnO_2 (C/M) core–shell fiber structure were fabricated with high electrochemical performance such as high rate capability with a scan rate up to 20 V s^{-1}, high volume capacitance of 2.5 F cm^{-3}, and an energy density of 2.2 × 10^{-4} Wh cm^{-3}. By integrating with a triboelectric generator, supercapacitors could be charged and power commercial electronic devices, such as a liquid crystal display or a light-emitting-diode, demonstrating feasibility as an efficient storage component and self-powered micro/nanosystems.

KEYWORDS: carbon · MnO_2 · core–shell fiber · supercapacitor · energy storage

A rapid development of flexible electronics such as roll-up displays, hand-held portable devices, and sensor networks have promoted the needs for flexible and lightweight energy sources.[1−10] Supercapacitors (SCs), which are superior in power density, long cycle life, and fast charge–discharge rates, have demonstrated feasibility as outstanding storage components.[7,11−13] Compared with the SCs using liquid electrolyte, all-solid-state SCs have many advantages such as lightweight, high flexibility, high safety and environmentally benign nature, which are suitable for flexible and portable electronics.[14−16]

Owing to the nature of flexible electronics, the corresponding power sources should not add too much size and weight. Benefited from its small size, flexibility, high conductivity, and large surface area, carbon fiber (CF) can serve as a good scaffold to load active materials and fabricate small size, lightweight and flexible SCs, which are important for biosensors, medical monitoring, and military projects. Owing to the low-cost, environmentally benign nature, and high specific capacitance, manganese oxide (MnO_2) is considered a good candidate material for high performance SCs.[17−19]

Herein, we fabricated all-solid-state SCs based on a C/M core–shell fiber structure, the CF served as a scaffold and current collector, and MnO_2 was deposited through a low-cost redox process.[14] The device showed high rate capability with a scan rate up to 20 V s^{-1}, a high volume capacitance of 2.5 F cm^{-3}, and an energy density of 2.2 × 10^{-4} Wh cm^{-3}. Moreover, the SCs integrated with a triboelectric generator (TG) could power a commercial liquid crystal display (LCD) or a light-emitting-diode (LED), demonstrating various potential applications for self-powered nanotechnology.

RESULTS AND DISCUSSION

The fabrication process of C/M core–shell fibers is illustrated in Figure 1a. The reaction between CF and $KMnO_4$ was achieved by following process:[20]

$$4MnO_4^- + 3C + H_2O \leftrightarrow 4MnO_2 + CO_3^{2-} + 2HCO_3^- \quad (1)$$

MnO_4^- reacted with CF and formed MnO_2 which covered the surface of CF, resulting in a C/M core–shell fiber. Figure 1panels b and c show scanning electron microscopy (SEM) images of an as-prepared and a broken C/M core–shell fiber, respectively, revealing the core–shell character of the fiber and indicating that the MnO_2 layer was deposited around CF. The microstructure

* Address correspondence to jun.zhou@mail.hust.edu.cn.

Received for review August 5, 2012 and accepted September 14, 2012.

Published online September 15, 2012
10.1021/nn303530k

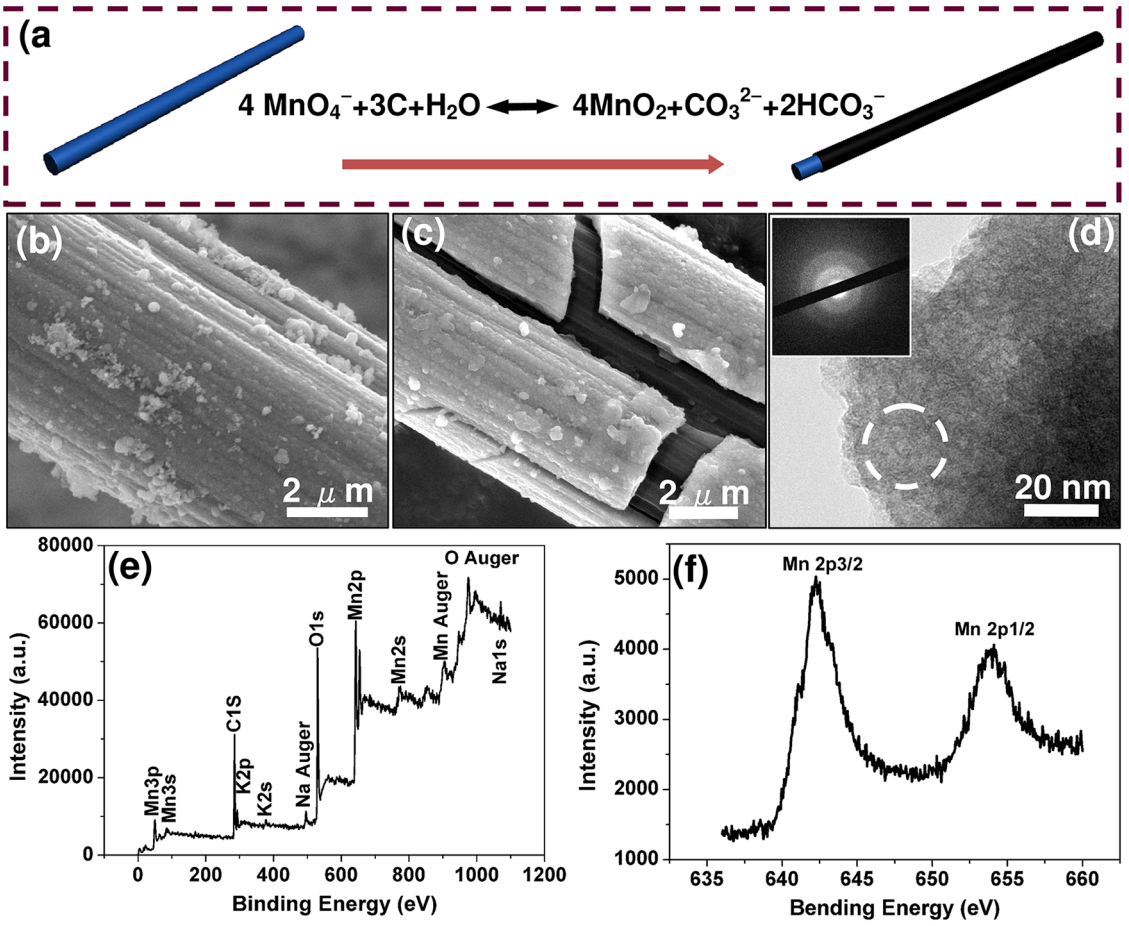

Figure 1. (a) Schematic of the growth process of C/M core–shell fiber structure. (b and c) SEM images of the as prepared and broken C/M core–shell fiber, respectively. (d) High magnification TEM images of MnO_2. (e and f) XPS spectrum of C/M core–shell fiber and Mn 2p level.

of the outer layer was characterized using transmission electron microscopy (TEM). Figure 1d showed a typical high resolution TEM image and the corresponding selected area electron diffraction (SAED) pattern of the outer layer, indicating that the outer layer was dominated by an amorphous phase. Energy dispersive X-ray spectroscopy (EDS) analysis was conducted from the dashed circle area of the outer layer (Figure S1). Besides Cu and C signals coming from the TEM grid, Mn, O, and K were detected in the sample; the K signal might come from the $KMnO_4$ precursor. The detailed chemical composition of as-prepared sample was probed by X-ray photoelectron spectroscopy (XPS) as shown in Figure 1e and 1f. There were five elements (Mn, C, K, Na, and O) present on the surface of the product. The C signal was attributed to carbon fiber and adventitious carbon; K and Na signals were attributed to $KMnO_4$ and Na_2SO_4 precursor, respectively. According to the Mn 2p spectrum (Figure 1f), two strong peaks centered at 642.3 and 654.1 eV corresponding to Mn^{4+} oxidation state were found.

To explore the electrochemical performance of the C/M core–shell fiber structure, we fabricated an all-solid-state SC, and the schematic of SC was shown in the inset of Figure 2a. Two C/M core–shell fibers were placed onto polyester (PET) substrate in parallel and H_3PO_4/poly (vinyl alcohol) (PVA) was used as the solid-state electrolyte. The volume of the two fibers was $\sim 1 \times 10^{-6}$ cm^3 (the fiber was considered as a cylinder, roughly, the volume of the device which included the fibers and electrolyte was $\sim 3 \times 10^{-5}$ cm^3), and all of the measurements were based on the volume of core–shell fibers. Electrochemical performance was analyzed by cyclic voltammetry (CV) scans at scan rates from 10 m V s^{-1} to 200 V s^{-1}. The CV area of C/M core–shell structure was much larger than that of CF as seen in Supporting Information, Figure S2. The CV curves retained their almost rectangular shape with little variance even at an ultrafast scan rate of 50 V s^{-1} as shown in Supporting Information, Figure S3. The discharge current showed a linear relationship with scan rates up to 20 V s^{-1} as seen in Figure 2d**.** This value revealed the fast charge transport which was significantly important for SCs.[2,21−24]

Galvanostatic charge–discharge and electrochemical impedance spectroscopy (EIS) measurements were performed to further evaluate the electrochemical performance of all-solid-state SCs. Typical galvanostatic charge–discharge curves were shown in Figure

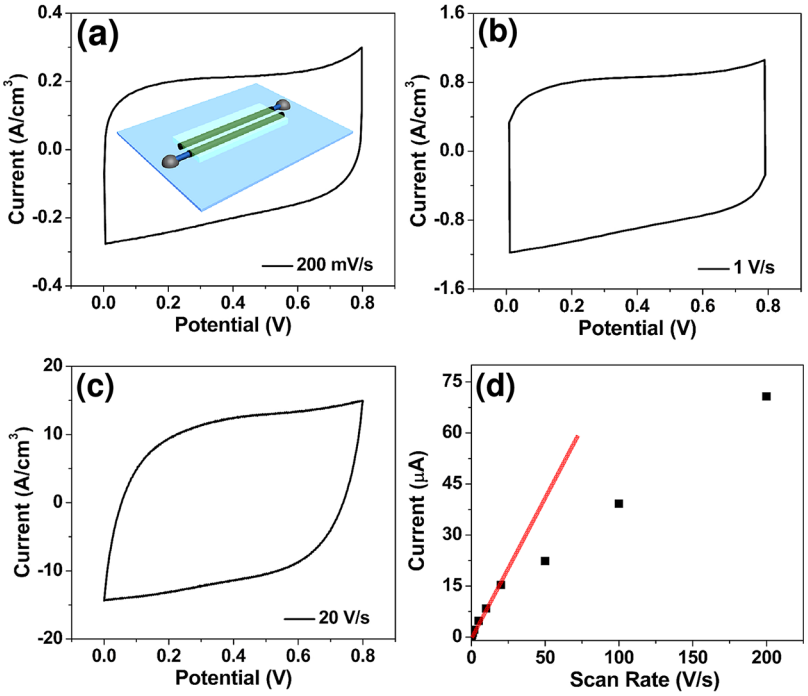

Figure 2. (a–c) CV curves at different scan rates. The schematic of the single SC device was shown in the inset of panel a. (d) Evolution of the discharge current versus scan rate.

3a, through which good linear voltage–time profiles were achieved, demonstrating a good capacitance performance. According to the EIS measurement, the straight line nearly paralleled to the imaginary axis, revealing an ideal capacitive behavior. The equivalent series resistance (ESR) of all-solid-state SC was as small as 2 mΩ cm^3 (Figure 3b). The maximum phase angle is about −81°, close to −90° for an ideal capacitor as can be seen in bode plot of Supporting Information, Figure S4. The real and imaginary parts of capacitance change with respect to frequency were shown in Figure 3c. The capacitor response frequency of f_0 was about 45 Hz and the relaxation time constant τ_0 is calculated to be about 22 ms by the equation $\tau_0 = 1/f_0$, which is even lower than SCs in liquid electrolyte.[2,25] The volume capacitance of the SC could be achieved by the following equations:

$$C = I\Delta t/\Delta E \quad (2)$$

$$C_v = C/V = I\Delta t/V\Delta E \quad (3)$$

where C is the total capacitance, I is the discharge current, Δt is the discharge time, ΔE is the potential window during the discharge process after IR drop, and V is the volume of the fibers. The highest volume capacitance was ~2.5 F cm^{-3} at 0.02 A cm^{-3} which was much higher than those reported in literature[2,18,26,27] and remain at 1.5 F cm^{-3} at 1 A cm^{-3}, demonstrating a good rate capability (Figure 3d). Moreover, the volume capacitance was consistent with the value achieved in Figure 3c. A Ragone plot showing the energy density with respect to the average power density of fabricated all-solid-state SCs as can be seen in Figure 3e. The energy density and average power density of the cell could be calculated following the equations:

$$E = 0.5C\Delta U^2/V \quad (4)$$

$$P = 3600E/\Delta t \quad (5)$$

where C was the total capacitance of the cell which can be achieved through eq 2, ΔU was the cell voltage, V was the volume of the fibers, and Δt was the discharge time. The highest energy density of the SC was 2.2×10^{-4} Wh cm^{-3} which was even comparable with graphene oxide and onion-like carbon SCs in liquid electrolyte.[2,28] In addition, the power density was obtained of 0.4 W cm^{-3} while the energy density was still 1.2×10^{-4} Wh cm^{-3}. For practical applications, cyclic stability was a crucial factor. As shown in Figure 3f, the device showed a stable cycle life between 0 and 0.8 V at 0.1 A cm^{-3} and remained at 84% of the initial capacitance after 10000 charge–discharge cycles. The discharge curves remained symmetric with charge counterparts and displayed good linear voltage–time profiles after cycling 10000 times (the inset in Figure 3f).

For application consideration, flexible and portable electronics may require highly flexible power sources working at different operation voltages and powers. The effect of curvature on the performance of the SC was examined by the following method. The PET substrate with SC on it was placed on two X–Y–Z mechanical stages with a moving step of 2 μm, and each end of the substrate was fixed on one stage by scotch tape. The bend angle of the substrate was controlled by adjusting the stages. We checked CV curves of the SC under five different bending angles

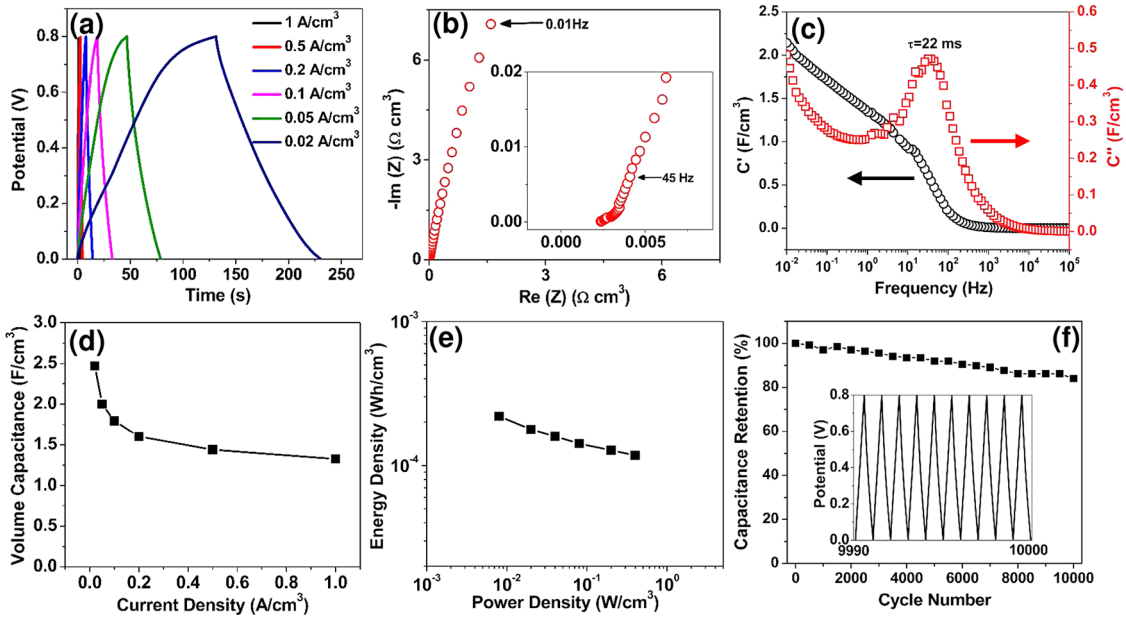

Figure 3. Electrochemical performance of single SC device. (a) Galvanostatic charge–discharge curves. (b) and (c) C′ and C″ plots of a single SC device. (d) Volume capacitance with respect to scan rates. (e) Ragone plot. And (f) Cycle life. The inset was the Galvanostatic charge–discharge curve after 10000 cycles.

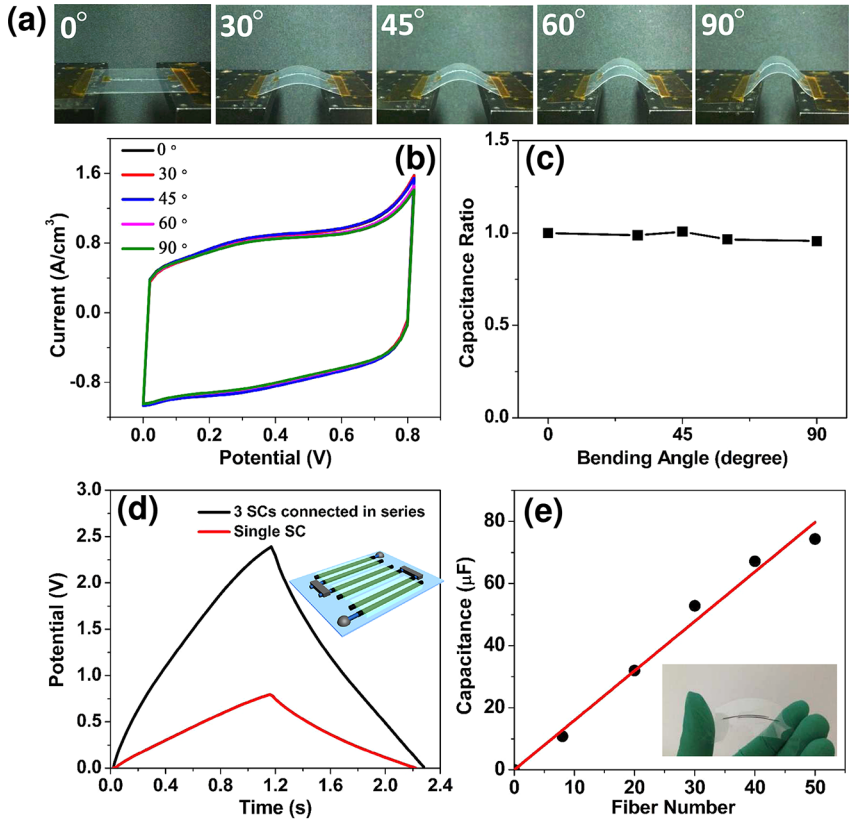

Figure 4. (a) Optical images of SCs bended with different angles. (b) CV curves of SCs bended with different angles. (c) Capacitance ratio for SCs with different angles. (d) Galvanostatic charge–discharge curves of single SC and three SCs connected in series. The inset showed the schematic of the three SCs connected in series. (e) Capacitance with respect to C/M core–shell fiber numbers to demonstrate the device could be scale-up. The inset was the optical image of a SC fabricated with 50 C/M core–shell fibers.

(0°, 30°, 45°, 60°, and 90°), which were shown in Figure 4a. No apparent change of the CV curves of SC were observed (Figure 4b) and the capacitance ratio remained ~1 (Figure 4c), revealing that the

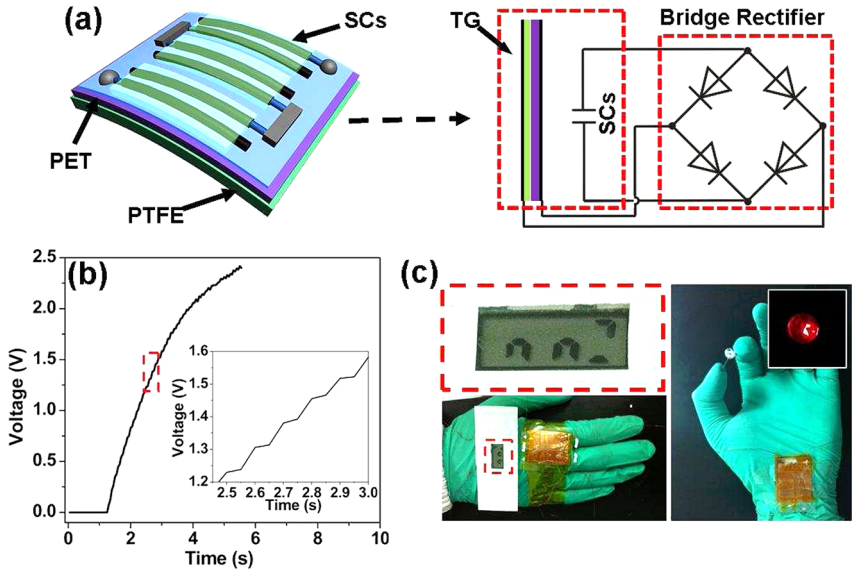

Figure 5. (a) Schematic diagram of energy modulus which is integrated by three SCs connected in series and a triboelectric generator. (b) Charging curve of three SCs connected in series charged by a triboelectric generator. The inset was an enlarged charging curve to show the voltage was step increased with the movement of hand. (c) Digital photograph of the energy modulus that is powering commercialized LCD (left) and LED (right).

electrochemical performance of the SC was hardly affected by the bending angle. To meet energy and power requirements, cells packaged either in series, in parallel, or in combinations of two may be the viable solution.[29] Developing an SC that would exhibit control over the operating voltage and capacitance by using serial and parallel assemblies would be an effective and energy-efficient way. Compared with a single SC, which operates at 0.8 V, the three SCs connected in series in our study exhibited a 2.4 V charge/discharge voltage window with almost the same discharge time (Figure 4**d**). The SCs connected in parallel was demonstrated by adding different number of C/M core–shell fibers (inset of Figure 4**e**). It should be noted that the capacitance showed a linear relationship with respect to the number of C/M core–shell fibers as shown in Figure 4**e**.

As efficient energy storage devices, SCs could be charged and then discharged to drive various commercial electronic devices. Specially, if SCs are integrated with a sustainable and renewable energy source, forming an energy module, they could make electronic devices work continually.[7,30] We have built an energy module to verify the feasibility of the SCs to store energy and power electronic devices as shown in Figure 5a. A TG[31,32] which was made of two sheets of polymers of polyethylene terephthalate (PET) and polytetrafluoroethylene (PTFE) was used to harvest energy. The output electric signals (voltage and current) were first rectified by a bridge rectifier, transforming alternating current (AC) to direct current (DC), and then the SCs were charged continually. We fixed the energy module on human hand and the SCs could be charged with the movement of the hand (see the Supporting Information, video 1). The charging curve of the three SCs connected in series was shown in Figure 5b. SCs could be charged to 2.4 V in around 5 s, and a step increased voltage signal can be clearly seen with each movement of hand (inset in Figure 5b). After the SCs were fully charged, the SCs could power commercial liquid crystal display (LCD) and light emitting diode (LED) as shown in Figure 5c.

SUMMARY

We reported all-solid-state SCs based on a C/M core–shell fiber structure. High electrochemical performance, such as high rate capability with the scan rate up to 20 V s^{-1}, a high volume capacitance of 2.5 F cm^{-3}, and energy density of 2.2 $\times$ 10^{-4} Wh cm^{-3}, was achieved. Moreover, high flexibility and easy scale-up property could be achieved, demonstrating potential applications for different operation voltages and energy demand. By integration with a TG, SCs could be charged and power commercial electronic devices such as LCDs and LEDs. By virtue of a environmentally benign nature, the devices demonstrate feasibility as efficient storage components and have potential applications for self-powered nanotechnology.

METHODS

Synthesis of C/M Core–Shell Fiber. MnO_2 was grown on CF *via* a self-limiting electroless deposition process reported previously.[17] Briefly speaking, 0.1 M $KMnO_4$ and 1 M Na_2SO_4 were mixed with equal volume. A bundle of CFs was immersed in the solution for 2 h at room temperature. Then the CFs were washed several times in deionized water.

Preparation of Solid-State SCs. The H_3PO_4/PVA gel electrolyte was prepared by mixing PVA powder (6 g), H_3PO_4 (6 g), and deionized water (60 mL) together. The mixture was heated to 85 °C with stirring until the solution became clear. The C/M core−shell fibers were closely and parallel located on a PET substrate with a separation space of ~1 mm, and an appropriate gel electrolyte was coated homogeneously on the fibers. The two electrodes were packaged spontaneous after the H_3PO_4/PVA gel solidified, and the solid state SC was prepared.

Preparation of Triboelectric Generator and Fabrication of the Energy Module. The TG was composed of two kinds of polymer. One was PET (3 × 2.3 cm) with a thickness of 220 μm and one side was covered with 100 nm ITO as the electrode. The other was PTFE (3× 2.3 cm) with 200 μm thickness and one side was covered by 200 nm Ti and 100 nm Cu as the electrode. Then two polymers were sealed with ordinary adhesive tape. To fabricate the energy module, the all-solid-state SCs were pasted on the triboelectric generator. The output from the generator was first rectified by a bridge rectifier, transforming alternating current (AC) to direct current (DC), and then connected to SCs.

Characterization. The morphologies, structure, and chemical composition of the products were characterized by high resolution field scanning electron microscopy (FEI Sirion 200), transmission electron microscopy (JEOL 4000EX), and X-ray photoelectron spectroscopy (XPS, ESCALab250). All of the electrochemical tests were carried out in a two-electrode system using Autolab PGSTAT302N. Electrochemical impedance was measured from 1 mHz to 1 MHz with a potential amplitude of 10 mV. A low-noise voltage preamplifier (model SR560, Stanford Research Systems, USA) and a sourcemeter (series 2400 SourceMeter, KEITHLEY) were used to measure the voltage−time and current−time curves.

Conflict of Interest: The authors declare no competing financial interest.

Acknowledgment. This work was financially supported by the National Natural Science Foundation of China (51002056, 51072236), a Foundation for the Author of National Excellent Doctoral Dissertation of PR China (201035), the Program for New Century Excellent Talents in University (NCET-10-0397). The authors thank the Analysis and Testing Center of Huazhong University of Science and Technology (HUST) and the Optoelectronic Micronano Fabrication Facility of Wuhan National Laboratory for Optoelectronics (WNLO). The authors also thank Mr. T. Zhai and Prof. Y. X. Tong from Sun Yat-sen University for their help.

Supporting Information Available: EDS analysis data of the outer layer from the dashed circle area in Figure 1d; CV curves of C/M core−shell and CF at 200 mV s^{-1}; CV curves of a single device at 50, 100, and 200 V s^{-1} scan rates; bode plot of a single SC device; video of the charging process of the SCs with the movement of the hand. This material is available free of charge *via* the Internet at http://pubs.acs.org.

REFERENCES AND NOTES

1. Simon, P.; Gogotsi, Y. Materials for Electrochemical Capacitors. *Nat. Mater.* **2008**, *7*, 845–854.
2. Pech, D.; Brunet, M.; Durou, H.; Huang, P.; Mochalin, V.; Gogotsi, Y.; Taberna, P. L.; Simon, P. Ultrahigh-Power Micrometre-Sized Supercapacitors Based on Onion-like Carbon. *Nat. Nanotechnol.* **2010**, *5*, 651–654.
3. Ihlefeld, J. F.; Clem, P. G.; Doyle, B. L.; Kotula, P. G.; Fenton, K. R.; Apblett, C. A. Fast Lithium-Ion Conducting Thin-Film Electrolytes Integrated Directly on Flexible Substrates for High-Power Solid-State Batteries. *Adv. Mater.* **2011**, *23*, 5663–5667.
4. Lipomi, D. J.; Vosgueritchian, M.; Tee, B. C.; Hellstrom, S. L.; Lee, J. A.; Fox, C. H.; Bao, Z. Skin-like Pressure and Strain Sensors Based on Transparent Elastic Films of Carbon Nanotubes. *Nat. Nanotechnol.* **2011**, *6*, 788–792.
5. Zhang, X.; Gong, L.; Liu, K.; Cao, Y.; Xiao, X.; Sun, W.; Hu, X.; Gao, Y.; Chen, J.; Zhou, J.; *et al.* Tungsten Oxide Nanowires Grown on Carbon Cloth as a Flexible Cold Cathode. *Adv. Mater.* **2010**, *22*, 5292–5296.
6. Xiao, X.; Yuan, L.; Zhong, J.; Ding, T.; Liu, Y.; Cai, Z.; Rong, Y.; Han, H.; Zhou, J.; Wang, Z. L. High-Strain Sensors Based on ZnO Nanowire/Polystyrene Hybridized Flexible Films. *Adv. Mater.* **2011**, *23*, 5440–5444.
7. Yuan, L.; Xiao, X.; Ding, T.; Zhong, J.; Zhang, X.; Shen, Y.; Hu, B.; Huang, Y.; Zhou, J.; Wang, Z. L. Paper-Based Supercapacitors for Self-Powered Nanosystems. *Angew. Chem., Int. Ed.* **2012**, *51*, 4934–4938.
8. Yang, Y.; Jeong, S.; Hu, L.; Wu, H.; Lee, S. W.; Cui, Y. Transparent Lithium-Ion Batteries. *Proc. Natl. Acad. Sci. U. S.A.* **2011**, *108*, 13013–13018.
9. Lu, X.; Wang, G.; Zhai, T.; Yu, M.; Gan, J.; Tong, Y.; Li, Y. Hydrogenated TiO_2 Nanotube Arrays for Supercapacitors. *Nano Lett.* **2012**, *12*, 1690–1696.
10. Yuan, L.; Lu, X. H.; Xiao, X.; Zhai, T.; Dai, J.; Zhang, F.; Hu, B.; Wang, X.; Gong, L.; Chen, J.; *et al.* Flexible Solid-State Supercapacitors Based on Carbon Nanoparticles/MnO_2 Nanorods Hybrid Structure. *ACS Nano* **2012**, *6*, 656–661.
11. Liu, J.; Jiang, J.; Cheng, C.; Li, H.; Zhang, J.; Gong, H.; Fan, H. J. Co_3O_4 Nanowire@MnO_2 Ultrathin Nanosheet Core/Shell Arrays: A New Class of High-Performance Pseudocapacitive Materials. *Adv. Mater.* **2011**, *23*, 2076–2081.
12. Lu, X.; Zhai, T.; Zhang, X.; Shen, Y.; Yuan, L.; Hu, B.; Gong, L.; Chen, J.; Gao, Y.; Zhou, J.; *et al.* WO_{3-x}@Au@MnO_2 Core−Shell Nanowires on Carbon Fabric for High-Performance Flexible Supercapacitors. *Adv. Mater.* **2012**, *24*, 938–944.
13. Stoller, M. D.; Ruoff, R. S. Best Practice Methods for Determining an Electrode Material's Performance for Ultracapacitors. *Energy Environ. Sci.* **2010**, *3*, 1294–1301.
14. Meng, C.; Liu, C.; Chen, L.; Hu, C.; Fan, S. Highly Flexible and All-Solid-State Paperlike Polymer Supercapacitors. *Nano Lett.* **2010**, *10*, 4025–4031.
15. Kaempgen, M.; Chan, C. K.; Ma, J.; Cui, Y.; Gruner, G. Printable Thin Film Supercapacitors Using Single-Walled Carbon Nanotubes. *Nano Lett.* **2009**, *9*, 1872–1876.
16. Weng, Z.; Su, Y.; Wang, D.-W.; Li, F.; Du, J.; Cheng, H.-M. Graphene-Cellulose Paper Flexible Supercapacitors. *Adv. Energ. Mater.* **2011**, *1*, 917–922.
17. Fischer, A. E.; Pettigrew, K. A.; Rolison, D. R.; Stroud, R. M.; Long, J. W. Incorporation of Homogeneous, Nanoscale MnO_2 within Ultraporous Carbon Structures *via* Self-Limiting Electroless Deposition: Implications for Electrochemical Capacitors. *Nano Lett.* **2007**, *7*, 281–286.
18. Yu, G.; Hu, L.; Vosgueritchian, M.; Wang, H.; Xie, X.; McDonough, J. R.; Cui, X.; Cui, Y.; Bao, Z. Solution-Processed Graphene/MnO_2 Nanostructured Textiles for High-Performance Electrochemical Capacitors. *Nano Lett.* **2011**, *11*, 2905–2911.
19. Hu, L.; Chen, W.; Xie, X.; Liu, N.; Yang, Y.; Wu, H.; Yao, Y.; Pasta, M.; Alshareef, H. N.; Cui, Y. Symmetrical MnO_2−Carbon Nanotube−Textile Nanostructures for Wearable Pseudocapacitors with High Mass Loading. *ACS Nano* **2011**, *5*, 8904–8913.
20. Jin, X.; Zhou, W.; Zhang, S.; Chen, G. Z. Nanoscale Microelectrochemical Cells on Carbon Nanotubes. *Small* **2007**, *3*, 1513–1517.
21. In, H. J.; Kumar, S.; Shao-Horn, Y.; Barbastathis, G. Origami Fabrication of Nanostructured, Three-Dimensional Devices: Electrochemical Capacitors with Carbon Electrodes. *Appl. Phys. Lett.* **2006**, *88*, 083104.
22. Pech, D.; Brunet, M.; Taberna, P. L.; Simon, P.; Fabre, N.; Mesnilgrente, F.; Conedera, V.; Durou, H. Elaboration of a Microstructured Inkjet-Printed Carbon Electrochemical Capacitor. *J. Power Sources* **2010**, *195*, 1266–1269.
23. Wang, K.; Zou, W.; Quan, B.; Yu, A.; Wu, H.; Jiang, P.; Wei, Z. An All-Solid-State Flexible Micro-supercapacitor on a Chip. *Adv. Energ. Mater.* **2011**, *1*, 1068–1072.
24. Sheng, K.; Sun, Y.; Li, C.; Yuan, W.; Shi, G. Ultrahigh-Rate Supercapacitors Based on Eletrochemically Reduced Graphene Oxide for AC Line-Filtering. *Sci. Rep* **2012**, *2*, 247.
25. Meng, F.; Ding, Y. Sub-Micrometer-Thick All-Solid-State Supercapacitors with High Power and Energy Densities. *Adv. Mater.* **2011**, *23*, 4098–4102.
26. Zhang, J.; Jiang, J.; Li, H.; Zhao, X. S. A High-Performance Asymmetric Supercapacitor Fabricated with Graphene-Based Electrodes. *Energy Environ. Sci.* **2011**, *4*, 4009–4016.

27. Pasta, M.; La Mantia, F.; Hu, L.; Deshazer, H. D.; Cui, Y. Aqueous Supercapacitors on Conductive Cotton. *Nano Res* **2010**, *3*, 452–458.
28. Gao, W.; Singh, N.; Song, L.; Liu, Z.; Reddy, A. L. M.; Ci, L.; Vajtai, R.; Zhang, Q.; Wei, B.; Ajayan, P. M. Direct Laser Writing of Micro-supercapacitors on Hydrated Graphite Oxide Films. *Nat. Nanotechnol.* **2011**, *6*, 496–500.
29. El-Kady, M. F.; Strong, V.; Dubin, S.; Kaner, R. B. Laser Scribing of High-Performance and Flexible Graphene-Based Electrochemical Capacitors. *Science* **2012**, *335*, 1326–1330.
30. Xiao, X.; Ding, T.; Yuan, L.; Shen, Y.; Zhong, Q.; Zhang, X.; Cao, Y.; Hu, B.; Zhai, T.; Gong, L.; *et al.* WO_{3-x}/MoO_{3-x} Core−Shell Nanowires on Carbon Fabric as Anode for All-Solid-State Asymmetric Supercapacitors. *Adv. Energ. Mater.* **2012**, 10.1002/aenm.201200380.
31. Fan, F. R.; Tian, Z.-Q.; Wang, Z. L. Flexible Triboelectric Generator. *Nano Energy* **2012**, *1*, 328–334.
32. Fan, F. R.; Lin, L.; Zhu, G.; Wu, W.; Zhang, R.; Wang, Z. L. Transparent Ttriboelectric Nanogenerators and Self-Powered Pressure Sensors Based on Micropatterned Plastic Films. *Nano Lett.* **2012**, *12*, 3109–3114.